Following the interstellar magnetic field from the heliosphere into space with polarized starlight

P C Frisch[1], A B Berdyugin[2], V Piirola[2], A M Magalhaes[3], D B Seriacopi[3], T Ferrari[3], F P Santos[4], N A Schwadron[5], H O Funsten[6], D J McComas[7], C E Heiles[8]

[1] Department of Astronomy and Astrophysics, University of Chicago, Chicago IL 60637 USA
[2] Tuorla Observatory and Finnish Centre for Astronomy with ESO, University of Turku, Finland
[3] Inst. de Astronomia, Geofisica e Ciencias Atmosfericas, Universidade de Sao Paulo, Sao Paulo, Brazil
[4] Center for Interdisciplinary Exploration and Research in Astrophysics and Department of Physics and Astronomy, Northwestern University, Evanston, IL 60208 USA
[5] Space Science Center, University of New Hampshire, NH 03824 USA
[6] Los Alamos National Laboratory, Los Alamos, NM 87544 USA
[7] Princeton Plasma Physics Lab, Princeton University, Princeton NJ 08543 USA
[8] Astronomy Department, University of California, CA 94720 USA

Abstract. Starlight linearly polarized by aligned interstellar dust grains provides the necessary data for tracing the structure of the very local interstellar magnetic field (ISMF). Two methods have been developed to recover the ISMF direction from polarized starlight, using data from an ongoing polarization survey. Both methods rely on the probability distribution function for polarized light. Method 1 calculates the ISMF direction from polarization position angles regardless of the data accuracy, while Method 2 relies on high-probability data points. The ISMF direction $B_{\rm IBEX}$ recovered by Method 1 corresponds to the closest ISMF to the heliosphere, traced by the center of the IBEX Ribbon arc. Method 2 reveals a new direction for the more distant ISMF, $B_{\rm new}$, toward ℓ=41.1° ± 4.1° and b= 25.8° ± 3.0°, which differs by 30.4° ± 5.6° from the IBEX ISMF direction. Polarizations of filament stars that are located within 25° of a pole of $B_{\rm new}$, where background polarizations would be minimal, show the highest statistical probabilities of tracing the filament ISMF. The IBEX ISMF direction orders the kinematics of interstellar clouds within 15 pc, and $B_{\rm new}$ must therefore dominate beyond 15 pc. These new data are consistent with the location of the Sun in the rim of an expanding superbubble shell associated with the evolved Loop I superbubble.

1. Introduction

Large-scale coherent magnetic features are found throughout the interstellar medium where they order synchrotron emission, rotate polarized radio emission, and organize the alignment of interstellar dust grains. At heliosphere scales of ∼ 0.001 pc the interstellar magnetic field (ISMF) direction is traced by the center of the Ribbon arc of energetic neutral atoms (ENAs) discovered by the Interstellar Boundary Explorer (IBEX) [1, 2, 3, 4, 5, 6]. Linearly polarized starlight provides the only currently available means for following the IBEX Ribbon ISMF from the heliosphere out into the low density interstellar gas in the immediate solar neighborhood. This linear polarization arises as starlight traverses a dichroic interstellar medium created by

charged dust grains that are aligned in the presence of a magnetic field [7, 8]. A survey is underway to map the structure of the local ISMF using polarized starlight, and connect the interstellar field to the magnetic field traced by the IBEX Ribbon. Previous results from this survey have been presented [9, 10, 11] and the new results are part of a broader study of the structure of the ISMF within 40 pc (Frisch et al. 2016 *in preparation*).

Two methods for obtaining the ISMF direction from the polarized starlight have been developed for use in this survey, one of which is sensitive to weak polarizations that may not alone be statistically significant [9, 10], and the other that builds the likely magnetic field directions from significant polarizations only and is presented for the first time in this paper (Section 2.2).

Three interstellar magnetic features stand out in the survey polarization data. The ISMF direction traced by the IBEX ENA Ribbon, $B_{\rm IBEX}$ [3], dominates the most weakly polarized stars within 40 pc and 90° of the heliosphere nose [9, 10]. These ENAs were created by charge exchange between interstellar neutral hydrogen atoms and energetic ions in directions that are perpendicular to the interstellar magnetic field draping over the heliosphere. The heliosphere nose direction corresponds to the upwind direction of interstellar neutral helium flowing into the heliosphere [12]. A nearby filamentary-shaped polarization feature was identified while searching for the ISMF direction associated with the IBEX Ribbon, leading to a more precise identification of the IBEX ISMF direction in the polarization data ([10, 11], Section 3). The filament shows geometrical properties related to the heliosphere, suggesting that the filament is the heliospheric version of the dusty bowshocks or bowwaves common around external stars [13]. A third magnetic field direction, $B_{\rm new}$, is traced by stronger polarizations.

These polarization survey data trace aligned interstellar dust grains in the cluster of local interstellar clouds. Additional features of the polarization data underlying the results in this paper are mentioned in Appendix A. The dominant local ISMF direction, which matches the IBEX Ribbon ISMF direction, orders the kinematics of nearby interstellar gas [10] and controls the flux of TeV galactic cosmic rays into the heliosphere [14]. Early measurements of the nearby interstellar magnetic field were puzzling, with disagreement between studies [15, 16]. A better understanding of the partially ionized magnetoionic medium through which the Sun is now traveling should emerge from the data provided by this survey.

2. Recovering Magnetic Field Directions from Optical Polarization Data

Optically polarized starlight forms as light traverses a dichroic medium created when optically asymmetic interstellar dust grains become aligned with respect to the interstellar magnetic field. Dissipation of grain angular momentum aligns the principle axis of inertia with the angular momentum vector, so that the spinning charged grains become aligned with respect to the ISMF direction [7, 8]. The consensus view is that grains are aligned so that the axis of lowest optical opacity, and therefore the polarization position angle PA of the linearly polarized starlight E-vector, is parallel to the ISMF direction. This assumption is the basis of our efforts to infer the ISMF direction from optically polarized starlight.

Approximately 1% of the mass of an interstellar cloud is carried by the dust grains. Typical column densities in the immediate solar neighborhood are $N(H^o) \leq 10^{18.5}$ cm^{-2} [17], leading to interstellar polarization strengths of 0.01%–0.02% using standard relations between color excess and $N(H^o)$, and polarization strength and color excess [10]. Sensitive measurements of the linear polarizations of nearby stars therefore provide a viable tool for tracing the spatial configuration of the local interstellar magnetic field.

Low local column densities, a patchy ISM distribution [17] that also includes dense clouds [18], and an inhomogeneous population of dust grains [17], lead to detections of significant polarizations that depend on both polarimeter sensitivity and the interstellar material. These survey polarization data are a combination of early (20th century) polarization data with relatively large mean errors and recent (21st century) polarization measurements, some with

mean errors $3\sigma < 0.01\%$.

2.1. Method 1: Minimize weighted polarization position angles in an ensemble of data
The first method that we established for finding the ISMF direction from a set of interstellar polarization PA data is based on creating a merit function that tests for goodness-of-fit of the PA data to an ISMF direction, and then evaluating that merit function for each possible ISMF direction on the sky to determine the ISMF direction that provides the best match to the weighted polarization data [9, 10]. The sine of a polarization position angle will be zero when evaluated in a coordinate system where the pole is rotated to coincide with the true interstellar magnetic pole. The advantage of this merit function is that data with all levels of signal-to-noise are utilized to determine the local ISMF direction, which is useful because of the low local column densities. Data are weighted with a probability distribution function (PDF) suitable for polarization position angles. Additional information about the statistical techniques of Method 1 can be found in Appendix B and Frisch et al. [10].

The best-fitting ISMF direction to polarization data for stars within 90° of the heliosphere nose and 40 pc (termed here the "studied region") was obtained using Method 1 for two separate fittings [10]. The first fit included all stars in this spatial region while the second fit excluded the filament stars (Section 3). The second fit provided the best match to the direction of the ISMF traced by the IBEX Ribbon and yielded an ISMF direction toward ℓ,b= $36.2°, 49.0°$ ($\pm 16°$). This fitting is sensitive to the large number of low-probability data points, that together place significant constraints on the merit function. The PDF for survey polarizations that trace the direction of the IBEX Ribbon ISMF is shown in Figure 1, right. The weighted center of the IBEX Ribbon is toward ecliptic coordinates $\lambda, \beta = 219.2° \pm 1.3°, 39.9° \pm 2.3°$ [3], or galactic coordinates $\ell, b = 34.8° \pm 4.3°, 56.6° \pm 1.2°$ [10]. These two ISMF directions are in agreement. There are a large number of data points with large mean errors, $P/dP <$ 2.0 (for polarization P with mean error dP), and low probabilities of matching the IBEX Ribbon ISMF direction, but these low-probability data points form smooth shoulders on the distribution with higher probabilities than the predicted probabilities from a statistically random probability distribution.

2.2. Method 2: Map most probable magnetic poles across the sky
An alternate method for obtaining the ISMF direction from linear polarization is to build the result directly from the PDF (Figure 1) by comparing polarization position angles rotated into the new coordinate system, $PA_{\rm coord}$, where the pole is aligned with a possible ISMF direction, and then counting the number of data points with statistical probabilities $p_{\rm s}$ larger than an arbitrary minimum value, $p_{\rm s} > p_{\rm min}$=0.5 for example. The coordinate system rotation with the most number of rotated polarization position angles with $PA_{\rm coord} > p_{\rm min}$ then defines the best-fitting ISMF direction. Effectively Method 2 draws a horizontal line through the PDF in Figure 1 and then selects the data points above that line for the analysis. Method 2 therefore ignores the more numerous low-probability data points, $p_{\rm min} < 0.5$, while identifying the ISMF directions traced by the strongest polarizations in the sample. Method 2 is particularly useful for yielding new insights into the filament of dust around the heliosphere ([10, 11], Section 3).

3. Evidence for dust filament around heliosphere
An unexpected result of the polarization survey was the identification of a polarization filament with properties related to the heliosphere geometry [11]. Filament stars were originally selected from the polarization data based on a marginal correlation between polarization position angles and star distance [9] that did not survive testing with a larger set of polarization data [10]. The larger data set instead showed that the filament polarizations are seen toward sixteen stars that

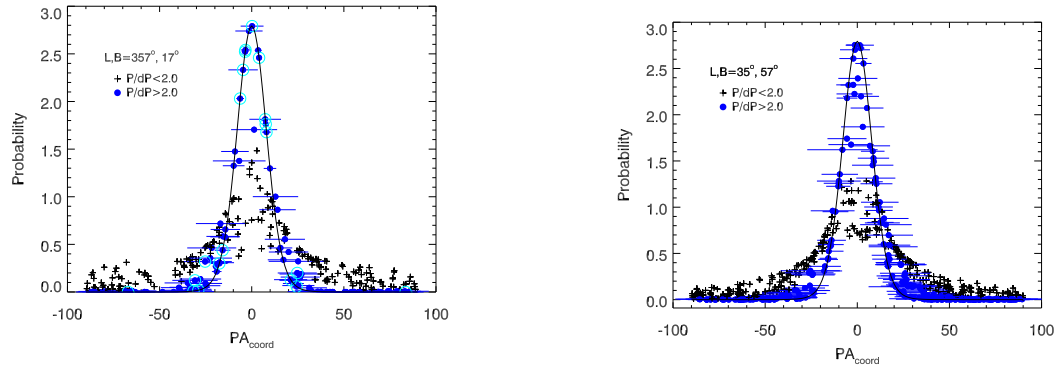

Figure 1. Probabilities that polarization position angles are aligned with the "true" ISMF direction. $PA_{\rm coord}$ is the polarization position angle expressed in a coordinate system where the magnetic pole is aligned with the true ISMF pole so that $PA_{\rm coord}$=0 for perfectly aligned grains. Left: Polarization position angles are expressed in a coordinate system aligned with the dust filament magnetic pole (ℓ=357°, b=17°). Solid lines show the underlying statistical probability distribution function for $P_{\rm o}$ = 3.5 (Appendix B). Blue dots (black crosses) indicate data where $P/dP>$ 2.0 ($<$ 2.0). Cyan-colored circles surround the filament stars. Right: The coordinate system pole and ISMF direction correspond to the ISMF direction traced by the center of the IBEX Ribbon ISMF arc (ℓ=35°, b=57°).

cover an angular extent of $\sim 100°$ and include three stars within 10 pc. Calculating the ISMF direction traced by the filament polarizations using Method 1 yielded a field direction toward galactic coordinates $\ell, b = 357.3°, 17.0°$. This direction is within $6.7° \pm 11.2°$ of the heliosphere nose direction given by the velocity vector of interstellar neutral helium entering the heliosphere and suggests that the filament is associated with the heliosheath region. Figure 2 shows the filament polarizations plotted in galactic coordinates in a stereographic projection (left), and a linear projection (right) that display other landmarks of the heliosheath region including the IBEX Ribbon [1, 19, 3].

Method 1 was originally applied to all polarization survey position angle data for the region under study, giving an ISMF direction offset by $32.4° \pm 16.6°$ from IBEX Ribbon ISMF direction. After the filament star subsample was identified and omitted from the calculations, the ISMF directions indicated by the polarization data and IBEX Ribbon agreed, differing by $7.6° \pm 16.6°$. The improved agreement between the polarization ISMF direction and the IBEX Ribbon ISMF found with omission of the filament stars from the sample supports a conclusion that the filament is a real magnetic structure in space.

Another filament property suggesting a heliosphere connection is that the axis of the filament is perpendicular to the heliosphere symmetry plane, the B-V plane, which is created by the velocity V of interstellar gas with respect to the Sun, the interstellar magnetic field direction B, and the Sun. Heliosphere symmetries about the B-V plane arise from Lorentz forces on charged particles that deflect charged plasma and particles in directions perpendicular to the magnetic field and particle velocities (e.g. [21, 22]). A linear fit to the filament axis yields an angle of $80° \pm 14°$ between the filament axis and the direction defined by the interstellar He velocity vector and IBEX ISMF pseudo-vector [11].

The scenario suggested here is that the filament polarizations are seen where the ion flow becomes fully deflected in the outer heliosheath regions and the flows of primary and secondary interstellar particles are beginning to diverge. In this region the ISMF direction and the gas velocity become parallel and are close to the heliopause.

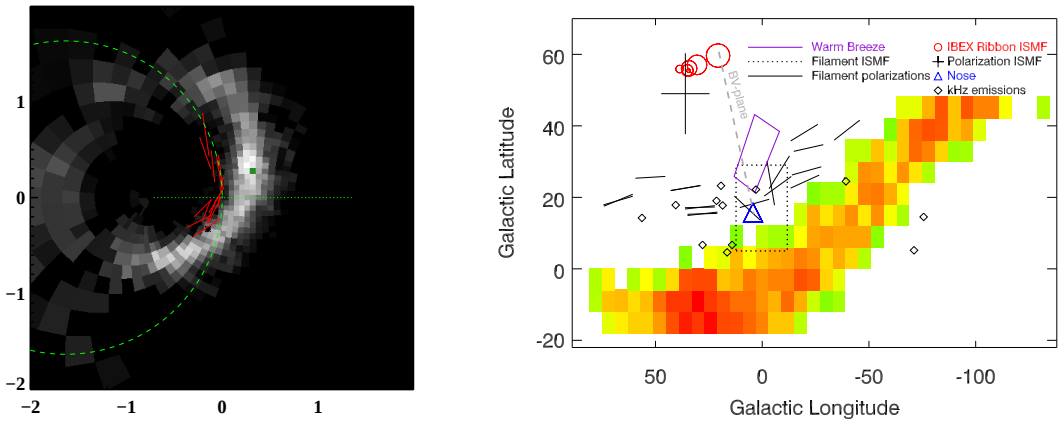

Figure 2. Left: A stereographic projection of the polarizations of the filament stars together with the brightest parts of the 1.1 keV IBEX Ribbon plotted in galactic coordinates. The scaling is nonlinear with a distance of 90° between labels 0 and 1, and 127° between labels 0 and 2. Longitude increases counterclockwise around the Ribbon arc. Right: The polarizations of the filament stars (black bars) are compared to markers of the outer heliosheath region or beyond. Uncertainties on the ISMF traced by the filament, which is toward the inflowing direction of interstellar helium wind, are outlined with a dotted box. The ISMF directions from the centers of the IBEX ribbon arc for the five energy bands of IBEX-HI [3] are plotted as red open circles, with the size of the circle increasing with energy. The black diamonds shows the locations of the outer heliosheath 2–3 kHz emissions [20]. The ISMF direction found from Method I applied to the polarization data is the large black cross. Dashed and solid gray lines show the locations of the B-V plane and the axis of the filament, respectively, which differ by an angle of $80° \pm 14°$. The IBEX Ribbon is shown for 1.1 keV data. See [11] for additional information.

The motion of the Sun through the surrounding low density weakly ionized interstellar cloud drives a flow of neutral or weakly charged interstellar gas and dust particles through the heliosphere. Enhanced charging of small grains in the hot heliosheath regions trap small grains with large charge-to-mass ratios in the plasma deflected around the heliosphere, where the interstellar grains that form the filament would be present [23, 24, 25]. Decades of *in situ* measurements of the mass distribution of interstellar dust grains by spacecraft confirm the exclusion of low-mass grains from the heliosphere [23, 26, 27] and indicate they have a silicate composition [28, 29], as is required by grain alignment scenarios [8] and predicted by abundance patterns of interstellar gas in the Local Interstellar Cloud (LIC) surrounding the heliosphere [30].

Low rates of collision between the interstellar grains and gas prevent collisional disruption of the coupling between grains with high charge-to-mass ratios and the ISMF. Voyager 1 entered the outer heliosheath at a distance of 124 AU [31], and found a non-turbulent ordered ISMF with a strength of ~ 4.7 μG for the interstellar field compressed against the heliopause [32]. The temporal variation of the ISMF direction detected by the magnetometer on Voyager 1 (presently located 30° north, at higher ecliptic latitude, of the heliosphere nose) is converging to the ISMF direction traced by the center of the IBEX ENA Ribbon [33]. The laminar characteristic found

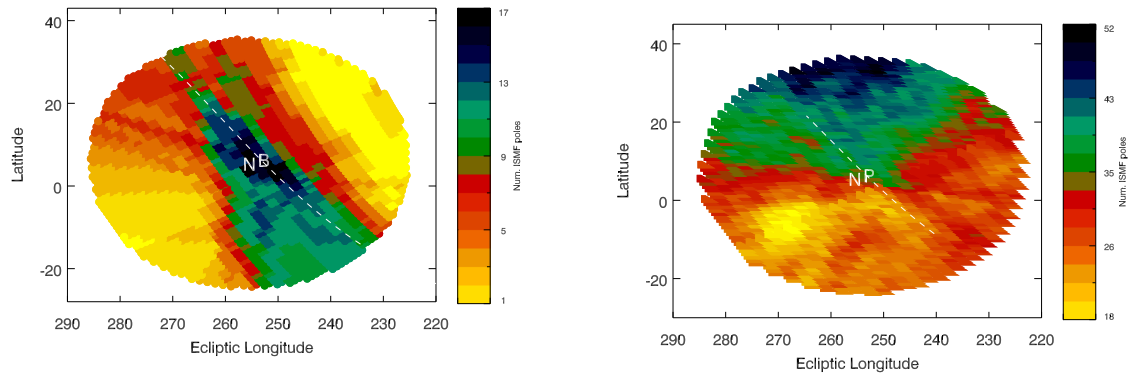

Figure 3. Left: The range of possible ISMF direction allowed by the polarizations of the filament stars is plotted in ecliptic coordinates. The number of polarizations with magnetic poles directed toward each location was calculated from Method 2 using probabilities larger than 0.5 for the PDF (Figure 1). The dashed line shows the best fit to the filament axis from [11], and the "B" marks the direction of the filament polarization obtained from Method 1. The "N" shows the heliosphere nose direction. The filament polarizations provide a well-defined parameter space for the filament ISMF direction. Right: Same as the left figure except that all stars within 40 pc and 85° of the heliosphere nose in the polarization catalog are included in the search for the number of data points that predict a magnetic pole for each location. Figure 1, left, explains the absence of the filament feature in the larger data set above-right since few stars have position angles directed toward the heliosphere nose.

by Voyager 1 for the ISMF in the outer heliosheath signifies the orderly draping of the ISMF over the heliosphere [34, 35] that would be required for a filamentary structure to form. Bending of the interstellar magnetic field-lines around the heliopause create the condition where the ISMF direction and therefore polarization position angles are parallel to the deflected currents that flow away from the heliosphere nose. Such a scenario might explain the existence of a polarizing dust filament around the heliosphere.

Theoretical simulations of interstellar dust grains interacting with a 3D MHD heliosphere predict that small charged dust grains, excluded from the heliosphere by the Lorentz force, create filamentary-like structures depending on the phase of the solar magnetic activity cycle [25]. These simulations show that dust grains interacting with the heliosphere experience forces that depend on solar cycle phase. The influence of the solar magnetic cycle has been shown to extend into the outer heliosheath and beyond, so that the filament might be a time-varying feature [36, 37].

A reasonable argument that the filament is a spurious effect could be made based on the fact that the nearest of the filament stars is 2500 times further away than the bowshock or bowwave of the heliosphere, at roughly 500 AU [38]. This is a valid concern because of the possibility that light from the filament stars is already polarized when it arrives in the heliosphere vicinity. The current data indicate that the filament stars with the largest statistical probabilities for tracing the filament ISMF direction, $p_s > 1.5$ (left figure of Figure 1), tend to be located within 25° of the direction of B_{new} and have low statistical probabilities for tracing B_{new}. The background polarization caused by B_{new} should therefore be weak because interstellar polarizations are weakest when sampling sightlines toward the ISMF direction. Polarizations arising from the background field B_{new} should be weaker by factors of ~ 2 or more for those filament stars with the largest probabilties of tracing the filament ISMF direction.

4. Probability distribution function for the IBEX ISMF direction

The direction of the ISMF field in the very local ISM was obtained by analyzing the best-fitting ISMF direction to the polarization data set, excluding the filament stars, using Method 1. Method 1 allows the large number of data points where the polarization is not detected at a statistically significant level to contribute to the result. Figure 1, right, shows the PDF for the polarization position angle values calculated with respect to the pole of the IBEX ISMF direction. It is apparent that even measurements with low statistical probability look like they are also sampling the IBEX ISMF direction. This is in contrast to the same distribution calculated for the filament stars (left, Figure 1) where the position angles of low probability data points do not look regularly distributed or as if they were sampling the filament ISMF direction.

The ISMF direction obtained with Method 1 is in agreement with the ISMF direction defined by the weighted mean center of the IBEX Ribbon ([3], see Section 3), and the large number of low probability measurements (Figure 1, right) is consistent with the very low column densities nearby.

The Ribbon models are still under debate [39]. Several variants of these models yield observational signatures measured near the Sun (e.g., at Earth) with energetic neutral atom fluxes predominantly from directions perpendicular to the local interstellar magnetic field draping over the heliosphere. The Ribbon properties have been simulated using MHD models of the ISMF draping over the heliosphere, with the production of ENAs seeded by secondary pickup ions that form upstream of the heliopause and produce preferred directions of ENA emission after charge-exchange with a neutral hydrogen atom [2, 4, 6]. These simulations predict an offset as large as $\sim 9^\circ$ between the center of the Ribbon arc and the ISMF direction far upstream of the heliopause.

4.1. Testing whether Method 1 and Method 2 give the same result for ISMF direction in the galactic center hemisphere

As a test we apply Method 2 to the whole polarization data set to see whether the result is the same as found from Method 1. The two methods inherently sample different parts of the PDF, with Method 1 also responding to low probability measurements and Method 2 counting only high-probability data points by definition (see Figure 1). Both methods utilize stars at any location in the region of study for the evaluation of the best-fitting ISMF. Figure 4, left, shows the number of stars within 40 pc and 85° (stet) of the heliosphere nose, with $P/dP > 2.0$ and a probability > 1.0 for polarization position angle to trace a magnetic pole at each location in the plotted region.

The longitude and latitude of the most probable magnetic pole is considered the location of the maximum number of probable position angles. For $p_s > 1.0$, the maximum number of position angles at any location is 34, and this maximum is found at five separate locations. Averaging the coordinates of these five locations together gives $\ell = 41.1^\circ \pm 4.4^\circ$ and $b = 25.8^\circ \pm 3.0^\circ$ for this new magnetic field direction, $B_{\rm new}$ (see Frisch et al. 2016, *in preparation*, for additional information). The separation between this location and the IBEX Ribbon ISMF is $30.4^\circ \pm 5.6^\circ$. This maximum likelihood ISMF direction is a prominent feature in Figure 4 that suggests that the ISMF far beyond the heliosphere has a different orientation than the ISMF shaping the heliosphere. If the difference between $B_{\rm IBEX}$ and $B_{\rm new}$ is indicative of magnetic turbulence in the local ISM then the turbulence would on average represent changes in direction of $\sim 0.8^\circ$ per parsec. The IBEX ISMF is the ISMF around the heliosphere, and $B_{\rm new}$ which is traced by statistically stronger data, is likely to trace the ISMF much further away but within 40 pc. $B_{\rm new}$ is unsettlingly close to the direction of the solar apex motion [10]. and the topic of a separate study (Frisch et al. 2016, *in preparation*).

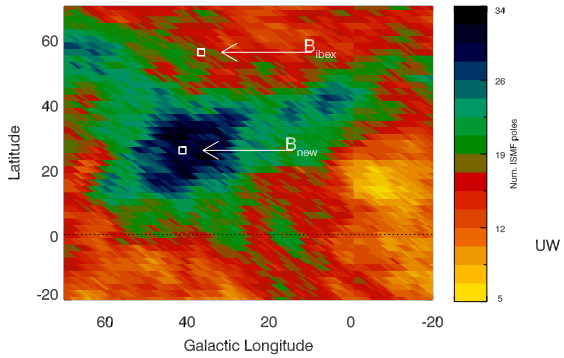

Figure 4. A section of the range of possible ISMF directions for the local ISMF direction as found by Method 2. The region that is displayed shows the most probable ISMF direction. The data in the figure represent measurements where $P/dP > 2.0$ and the probability of a polarization position angle tracing a magnetic pole at each location is $p_s > 1.0$ (see Figure 1). A new ISMF direction $B_{\rm new}$ appears as an excess of data points tracing a magnetic pole at ℓ=41.1° ± 4.1° and b= 25.8° ± 3.0° that is separated by 30.4° ± 5.6° from $B_{\rm IBEX}$.

A large semi-circular feature of unknown origin also appeared in the fourth galactic quadrant when Method 2 was applied to the position angle data in the studied region. This feature consists of preferred directions for the directions of polarization position angles, and therefore for magnetic field poles. Additional information about the polarization survey data is presented in Appendix A.

5. Influence of ISMF on local ISM

By three measures the dominant ISMF direction traced by the IBEX Ribbon orders the kinematics of nearby interstellar gas. The only interstellar cloud for which we have *in situ* measurements of both the cloud velocity and the ISMF direction is the LIC that surrounds the heliosphere. IBEX data on the interstellar helium velocity and the Ribbon ISMF direction show that the LIC velocity through the LSR is perpendicular to ISMF direction, with a relative angle of 87.3° ± 3.0° [40, 10].

A comparison between the individual kinematical groups used to model the interstellar gas within ∼ 15 pc [41] and the IBEX ISMF direction $B_{\rm IBEX}$ shows that interstellar cloud velocities through the LSR have a speed that increases with the angle between the IBEX ISMF direction and cloud velocity vector (Figure 5, [10]). This increase is not seen when cloud LSR velocity is compared with $B_{\rm new}$. $B_{\rm new}$ traces the strongest polarizations that are more likely to form further from the Sun, while the Redfield and Linsky model places the fifteen clouds within 15 pc. It is not surprising that $B_{\rm IBEX}$ rather than $B_{\rm new}$ orders the cloud speeds.

Longstanding measurements of nearby interstellar absorption lines towards the Sco-Cen Association region have indicated that the very local ISM flows away from the center of the Loop I superbubble [17]. Wolleben (2007, [42]) developed a quantitative model for the synchrotron emission as a composite of two superbubbles, with the "S1" shell being the most likely to affect the very local interstellar material. Figure 6 shows the fifteen local interstellar clouds [41] that are flowing away from the center of the Loop I superbubble (also see [43]). Berdyugin and Piirola [44] have shown that high-latitude polarized starlight traces the S1 shell, while Santos et al. [45] have shown that the entire region of Loop I is well-defined by polarization data. The Wolleben model places the nearside of the S1 shell at the solar location. The survey polarization data

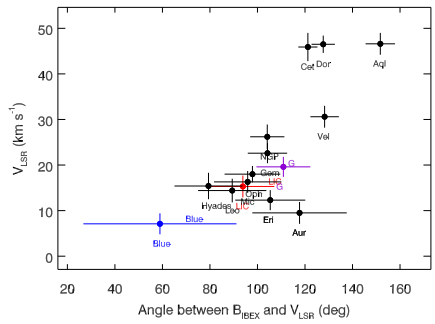

Figure 5. The angle between the LSR velocity of nearby interstellar clouds and the direction of the IBEX ISMF is shown plotted against the cloud speed. The ISMF direction is more disrupted for clouds accelerated to higher LSR speeds. Cloud names and velocities are based on the fifteen cloud local ISM model presented in [41]. The figure is from [10].

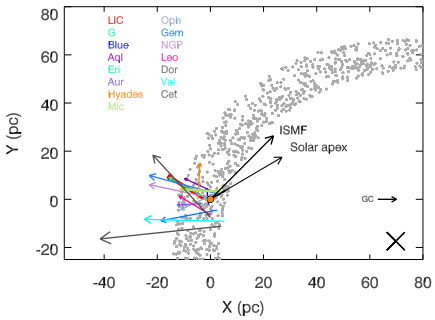

Figure 6. Cloud LSR velocities (arrows) are plotted over the S1 shell (gray dots) that describes synchrotron features associated with the Loop I superbubble centered at the "X", using the model of [42]. LSR cloud velocities are color coded. Black arrows show the directions of the IBEX ISMF direction and the solar apex motion through the LSR.

further support this interpretation, as does the fact that $B_{\rm new}$ and the IBEX Ribbon ISMF are directed toward different regions of the North Polar Spur that is the most prominent feature of Loop I. An alternate model that couples the local interstellar gas and ISMF models the detachment of a magnetic flux tube from the walls of the Local Bubble [46].

6. Conclusion

A survey is underway to probe the structure of the interstellar magnetic field within 40 pc using polarized starlight. Two methods are used to recover the ISMF direction from these data. Both methods rely on the statistical probabilities that a polarization position angle traces the "true" ISMF direction. Method 1 utilizes all suitable polarization data, regardless of uncertainties, while Method 2 selects only data with high probabilities for tracing a given field direction. Three ISMF directions are currently found from these data. The IBEX Ribbon ISMF direction that represents the ISMF closest to the heliosphere was found with Method 1, a new ISMF direction that is $30.4^\circ \pm 5.6^\circ$ away from $B_{\rm IBEX}$ was found with Method 2, and a third magnetic field direction toward the heliosphere nose is found to be traced by a filament of polarized starlight. Understanding the paleoheliosphere and astrospheres requires a full understanding of the ISMF direction in the surrounding interstellar medium. These polarization data are filling a gap in knowledge of the ISMF in the solar neighborhood.

Acknowledgments

This research has been supported by the NASA Explorer program through support for the IBEX mission and by the ERC Advanced Grant Hot-Mol ERC-2011-AdG-291659. AMM is grateful for support from FAPESP (grant no. 2010/19694-4) and CNP (Research Grant). DBS is grateful for support from CAPES (Phd scholarship). We are grateful to the Institute for Astronomy at the University of Hawaii (IfA) for the allocation of IfA time for observations at the T60 and UH88 telescopes, and to LNA, Brazil, for the allocation of observing time at the Observatorio do Pico dos Dias (OPD).

Appendix A. Polarization survey data

A survey is underway to map the structure of the local ISMF within 40 pc of the Sun using linearly polarized starlight. The results reported in this paper utilize data in the literature, data previously acquired specifically for this survey [9, 10, 11], and data recently acquired with the University of Hawaii UH88 telescope at Mauna Kea and the T60 telescope at Haleakala, and the Observatorio do Pico dos Dias (OPD), LNA, Brazil. The data utilized in the results reported in this paper were collected during the 20th and 21st centuries [9, 10, 11] and include new data (Frisch et al., 2016, *in preparation*).

Polarization data collected after the year 2000 are more accurate than data collected earlier due the higher accuracies of modern polarimeters [47, 48, 49, 50]. Polarization measurements of 755 stars provide the basis for the analysis in this paper. The mean value of P/dP for the 334 measurements collected after 2000 is 3.90. The mean value for 20th century measurements of P/dP is 1.60. The mean uncertainties for the 21st and 20th century data are 0.015% and 0.026% respectively.

Appendix B. Equations for evaluating polarization probabilities

A merit function has been utilized to extract the "true" ISMF direction from an ensemble of polarization position angles [10]. The goal of the merit function is to minimize the mean sine of the polarization position angles while weighting the data using a statistical distribution suitable for polarization data. The merit function is:

$$F_{\rm II}(B_{\rm i}) = {\rm N}^{-1} \sum_{\rm n=1}^{\rm N} f_{\rm n}(B_{\rm i}) = |\frac{\sin(\theta_{\rm n}(B_{\rm i}))}{G_{\rm n}}| \tag{B.1}$$

The contribution of each individual star n to the merit function for ISMF direction $B_{\rm i}$ is $f_{\rm n}(B_{\rm i})$. The quantity $\theta_{\rm n}(B_{\rm i})$ is the polarization position angle $PA_{\rm n}$ for star n, which is calculated with respect to the i$^{\rm th}$ possible interstellar magnetic field direction $B_{\rm i}$. The sum is over N stars with the statistical weighting function for each star given by:

$$G_{\rm n}(\theta_{\rm obs};\ \theta_{\rm o}, P_{\rm o}) \ = \ \frac{1}{\sqrt{\pi}} \ \{\frac{1}{\sqrt{\pi}} + \eta_{\rm o} \ \exp(\eta_{\rm o}^2) \ [1 + {\rm erf}(\eta_{\rm o})]\} {\rm exp}(-\frac{\rm P_o^2}{2}) \tag{B.2}$$

using the probability distribution for polarization position angles in Naghizadeh and Clarke (1993,[51]). The observed position angle is $\theta_{\rm obs}$, the "true" position angle is $\theta_{\rm o}$, and $P_{\rm o} = \frac{P_{\rm true}}{\sigma}$, mean error σ=dP, $\eta_{\rm o} \ = \ \frac{P_{\rm o}}{\sqrt{2}}$ cos $[2(\theta_{\rm obs} - \theta_{\rm o})]$, and the Gaussian error function $erf(Z) \ = \ \frac{2}{\sqrt{\pi}} \int_0^Z exp(-t^2)\ dt$.

This probability distribution function is non-gaussian because of the bivariate nature of the position angle and the fact that polarizations are always positive while the underlying Stokes parameters can be positive or negative; the PDF reverts to a Gaussian at large probabilities (> 6). Constraints are placed on some parameters to avoid introducing spurious results related to poor data or variations in observing techniques. See Frisch et al. (2015, [10]) for additional information.

References

[1] McComas D J, Allegrini F, Bochsler P et al. 2009 *Science* **326** 959
[2] Schwadron N A, Bzowski M, Crew G B et al. 2009 *Science* **326** 966
[3] Funsten H O, DeMajistre R, Frisch P C et al. 2013 *ApJ* **776** 30
[4] Heerikhuisen J, Pogorelov N V, Zank G P et al. 2010 *ApJ* **708** L126–L130
[5] Heerikhuisen J and Pogorelov N V 2011 *ApJ* **738** 29
[6] Zirnstein E J, Heerikhuisen J, Funsten H O, Livadiotis G, McComas D J and Pogorelov N V 2016 *ApJ* **818** L18

[7] Lazarian A 2007 *J. Quant. Spec. Radiat. Transf.* **106** 225–256
[8] Andersson B G, Lazarian A and Vaillancourt J E 2015 *ARA&A* **53** 501–539
[9] Frisch P C, Andersson B G, Berdyugin A et al. 2012 *ApJ* **760** 106
[10] Frisch P C, Berdyugin A, Piirola V et al. 2015 *ApJ* **814** 112
[11] Frisch P C, Andersson B G, Berdyugin A et al. 2015 *ApJ* **805** 60
[12] Schwadron N A, Moebius E, Leonard T et al. 2015 *ApJS* **220** 25
[13] Peri C S, Benaglia P, Brookes D P, Stevens I R and Isequilla N L 2012 *A&A* **538** A108
[14] Adams, F. C., Christian, E. R. et al 2014 *Science* **343** 988
[15] Tinbergen J 1982 *A&A* **105** 53–64
[16] Leroy J L 1993 *A&AS* **101** 551
[17] Frisch P C, Redfield S and Slavin J 2011 *ARA&A* **49**
[18] Peek J E G, Heiles C, Peek K M G, Meyer D M and Lauroesch J T 2011 *ApJ* **735** 129
[19] Schwadron N A, Allegrini F, Bzowski M et al. 2011 *ApJ* **731** 56–77
[20] Gurnett D A, Kurth W S, Allendorf S C and Poynter R L 1993 *Science* **262** 199
[21] Pogorelov N V, Heerikhuisen J, Mitchell J J, Cairns I H and Zank G P 2009 *ApJ* **695** L31–L34
[22] Opher M, Bibi F A, Toth G, Richardson J D, Izmodenov V V and Gombosi T I 2009 *Nature* **462** 1036–1038
[23] Frisch P C, Dorschner J M, Geiss J et al. 1999 *ApJ* **525** 492–516
[24] Kimura H and Mann I 1999 *Earth, Planets, and Space* **51** 1223–1232
[25] Slavin J D, Frisch P C, Müller H R, Heerikhuisen J, Pogorelov N V, Reach W T and Zank G 2012 *ApJ* **760** 46
[26] Landgraf M, Baggaley W J, Grün E, Krüger H and Linkert G 2000 *J. Geophys. Res.* **105** 10343–10352
[27] Sterken V J, Strub P, Krüger H, von Steiger R and Frisch P 2015 *ApJ* **812** 141
[28] Westphal A J and the Stardust Team 2014 *Science* **345** 786,791
[29] Altobelli N, Postberg F and et al 2016 *Science* **352** 6283
[30] Slavin J D and Frisch P C 2008 *A&A* **491** 53–68
[31] Gurnett D A, Kurth W S, Burlaga L F and Ness N F 2013 *Science* **341** 1489–1492
[32] Burlaga L F and Ness N F 2014 *ApJ* **784** 146
[33] Schwadron N A, Richardson J D, Burlaga L F, McComas D J and Moebius E 2015 *ApJ* **813** L20
[34] Pogorelov N V, Heerikhuisen J, Zank G P, Borovikov S N, Frisch P C and McComas D J 2011 *ApJ* **742** 104
[35] Opher M and Drake J F 2013 *ApJ* **778** L26
[36] Pogorelov N V, Suess S T, Borovikov S N, Ebert R W, McComas D J and Zank G P 2013 *ApJ* **772** 2
[37] Zirnstein E J, Funsten H O, Heerikhuisen J and McComas D J 2016 *A&A* **586** A31
[38] Zank G P, Heerikhuisen J, Wood B E, Pogorelov N V, Zirnstein E and McComas D J 2013 *ApJ* **763** 20
[39] McComas D J, Lewis W S and Schwadron N A 2014 *Reviews of Geophysics* **52** 118–155
[40] Schwadron N A, Adams F C, Christian E R, Desiati P, Frisch P, Funsten H O, Jokipii J R, McComas D J, Moebius E and Zank G P 2014 *Science* **343** 988–990
[41] Redfield S and Linsky J L 2008 *ApJ* **673** 283–314
[42] Wolleben M 2007 *ApJ* **664** 349–356
[43] Frisch P C 2010 *ApJ* **714** 1679–1688
[44] Berdyugin A, Piirola V and Teerikorpi P 2014 *A&A* **561** A24
[45] Santos F P, Corradi W and Reis W 2011 *ApJ* **728** 104
[46] Cox D P and Helenius L 2003 *ApJ* **583** 205–228
[47] Piirola V, Berdyugin A and Berdyugina S 2014 *Society of Photo-Optical Instrumentation Engineers (SPIE) Conference Series* (*Society of Photo-Optical Instrumentation Engineers (SPIE) Conference Series* vol 9147) p 8
[48] Wiktorowicz S J and Matthews K 2008 *PASP* **120** 1282–1297
[49] Magalhães A M, Pereyra A, Melgarejo R, de Matos L, Carciofi A C, Benedito F F C, Valentim R, Vidotto A A, da Silva F N, de Souza P P F, Faria H and Gabriel V S 2005 *Astronomical Polarimetry: Current Status and Future Directions* (*Astronomical Society of the Pacific Conference Series* vol 343) ed Adamson A, Aspin C, Davis C and Fujiyoshi T pp 305–+
[50] Bailey J, Kedziora-Chudczer L, Cotton D V, Bott K, Hough J H and Lucas P W 2015 *MNRAS* **449** 3064–3073
[51] Naghizadeh-Khouei J and Clarke D 1993 *A&A* **274** 968